Aperture optimization for emission imaging: effect of a spatially varying background

K. J. Myers

Center for Devices and Radiological Health, U.S. Food and Drug Administration, HFZ-142, 12720 Twinbrook Parkway, Rockville, Maryland 20857

J. P. Rolland and H. H. Barrett

Department of Radiology and Optical Sciences Center, University of Arizona, Tucson, Arizona 85724

R. F. Wagner

Center for Devices and Radiological Health, U.S. Food and Drug Administration, HFZ-142, 12720 Twinbrook Parkway, Rockville, Maryland 20857

Received October 18, 1989; accepted February 23, 1990

A method for optimizing the aperture size in emission imaging is presented that takes into account limitations due to the Poisson nature of the detected radiation stream as well as the conspicuity limitation imposed by a spatially varying background. System assessment is based on the calculated performance of two model observers: the best linear observer, also called the Hotelling observer, and the nonprewhitening matched-filter observer. The tasks are the detection of a Gaussian signal and the discrimination of a single from a double Gaussian signal. When the background is specified, detection is optimized by enlarging the aperture; an inhomogeneous background results in an optimum aperture size matched naturally to the signal. The discrimination task has a finite optimum aperture for a flat background; a nonuniform background drives the optimum toward still-finer resolution.

INTRODUCTION

An emission imaging system generally consists of an x-ray or gamma-ray source, an aperture element, and a detector. Radiation travels in a straight line from the object through the aperture, and a shadow of the object as seen through the aperture is cast onto the detector plane. A fundamental unsolved problem in planar emission imaging is that of specifying the optimal photon-collecting aperture. Large apertures yield high photon counts with great positional uncertainty or poor resolution. Conversely, small apertures yield small positional uncertainty or good resolution but with low photon counts. Clearly, there is a choice between resolution and collection efficiency that must be made each time a system is designed.

Finding the optimal trade-off between resolution and collection efficiency requires some quantitative specification of the performance of the imaging system. Early attempts in this direction focused on the calculation of the mean and the variance of the image, both of which, in general, depend on the object and its position in the image. A formalism called the noise kernel was developed from which these quantities as well as the noise autocorrelation function could be calculated. (For a review, see Barrett and Swindell.[1]) Results of these calculations are frequently given in terms of a position-dependent signal-to-noise ratio (SNR) or pixel SNR. This SNR may be interpreted as the reciprocal of the relative statistical error in an estimate of the object activity at each point. Though the noise-kernel formalism yields a complete statistical description of the image, at least through second-order statistics, it is nevertheless an incomplete statement of imaging system performance. The difficulty is that it is not clear how to relate the pixel SNR, or the statistical quantities that underlie it, to the performance of any specific task of interest.

A preferred approach to image assessment is to determine the performance of a model observer on some specified task. For example, there is considerable literature on the ideal or Bayesian observer, defined as one who has full knowledge of all relevant statistical properties of the images and of the task at hand and who uses that information in such a way as to minimize a suitably defined risk.[2,3] Bayesian theory gives a prescription for calculating the optimum strategy for a particular decision task. The model observer that carries out the optimum or Bayesian strategy is termed the ideal observer. For example, in cases that are both signal known exactly (SKE) and background known exactly (BKE) and for which the noise is additive and Gaussian, the ideal observer's strategy is readily shown to be equivalent to a prewhitening matched filter (PWMF). The performance of the ideal observer is easily calculated in this case and can therefore be used as a basis for system assessment and optimization. It is implicitly assumed in this approach that a system optimized for a model observer and an exactly specified task will also be optimal for the actual observer and for more realistic tasks. It is therefore of considerable practical importance to verify the validity of this assumption.

Consider the problem of aperture design when the task is the detection of a completely specified signal in an infinite uniform background of known strength. The ideal strategy

0740-3232/90/071279-15$02.00

for determining whether the signal is present in this task is to use a simple mask to estimate the number of photons in the image at the location of the expected object. Since the background level is exactly known, the observer can perform a statistical test to determine whether the number of detected counts in the region of the expected signal is consistent with the background level. When the number of detected counts is greater than the observer's threshold, a decision is made is favor of the signal's being present in the object. The larger the aperture, the more counts are collected from the signal region in the object, and hence the higher is the SNR of the signal count estimate. The complete background specification of this task results in an optimum aperture that is infinite in spatial extent.

In a generalization of the above task, Tsui *et al.*[4] calculated the performance of several model observers as a function of aperture size for the problem of detection of a spherical tumor in a finite uniform background of unknown strength. The realism of the problem was increased further by assuming a finite detector area. One observer model in the Tsui paper closely approximated the Bayesian strategy for the task. Because the flat background was known in only a statistical sense, the observer had to make an estimate of the background in an annular region about the signal and compare that with an estimate of the activity level at the location of the expected signal. The authors optimized the integration areas of the two regions of estimation for each aperture size that they considered. The uncertainty in the flat-background level, together with the finite image field, resulted in a finite optimum aperture size for the maximum observer SNR. In other words, spatial resolution was an important system design parameter for this task. When the background strength was assumed to be known, the authors found the optimum size of the aperture to increase to infinity, which is in keeping with the discussion in the paragraph above.

More recently, an interesting model problem was presented by Wagner *et al.*[5] They considered a high-contrast Rayleigh task in which the ideal observer was asked to determine whether a noisy scene was the image of a single or a double Gaussian signal. This discrimination task was suggested as a useful test of imaging system performance by Harris.[6] The task was a SKE/BKE task in that the width of the sources and the separation of the pair were known, as was the strength of the uniform background upon which they were superimposed. Both the background and the detector were assumed to have infinite spatial extent. Since the only randomness in the task was due to Poisson statistics, the formulation of the Bayesian decision strategy was straightforward. Using a signal-detection framework, Wagner *et al.* determined how ideal-observer performance varied as a function of source width and separation for three apertures: a simple pinhole, a large open aperture (twenty times the pinhole diameter), and a coded aperture that is known as the uniformly redundant array. They found that the ideal-observer performance was much better for the uniformly redundant array than for the small pinhole when the signal had high contrast. The ranking of the code and the large aperture depended on the source width and separation, with the large aperture outperforming the code for broad signals that were widely separated. The surprising conclusion of Wagner *et al.* was that the large aperture outperformed the simple pinhole for all source widths and separations.

The study of Wagner *et al.* suggests that, for certain tasks, a large open aperture is much better than a small pinhole, according to the calculated performance of the ideal observer. Yet, this conclusion does not seem to agree with current experimental practices in emission imaging. For example, in the field of nuclear medicine, spatial resolution (width of the point-spread function) of approximately 1 cm seems to give the best subjective image quality. It is the purpose of the present paper to further understand the source of this paradox.

The detection and Rayleigh studies that found superior performance for large apertures have two common features. One is the complete specification of the background and signal, and the other is the infinite size of the detector area. To resolve the apparent contradiction between the results of these studies and current experimental practice, we shall investigate tasks in which the signal is still known exactly but the background is permitted to vary randomly from image to image and have a spatially varying (lumpy) character. We shall show that even in the circumstance of infinite background and detector extent, a spatially varying background drives an imaging system to finite optimum resolution.

METHODS

In order for an imaging system to be evaluated objectively, the imaging system (bias, noise sources, etc.) must be specified, a task must be defined, and assumptions regarding the nature of the observer performing the task must be laid out. We describe these three steps in the sections that follow.

Image Formation

We shall be concerned with linear, shift-invariant imaging systems. The object in our simulations is a discrete representation of a two-dimensional function whose pixel values can be lexicographically ordered to form the $N \times 1$ column vector $\mathbf{f}$. We can represent the emission imaging system that we wish to optimize by the $M \times N$ linear operator $\mathbf{H}$. We can therefore write the imaging equation as

$$\mathbf{g} = \mathbf{H}\mathbf{f} + \mathbf{n}, \tag{1}$$

where the $M \times 1$ column vector $\mathbf{g}$ is the detected data and $\mathbf{n}$ is any noise in the data. The data vector $\mathbf{g}$ is random because of the Poisson nature of $\mathbf{n}$ as well as the statistical nature of the background inhomogeneity contained in $\mathbf{f}$. The system operator $\mathbf{H}$ contains the aperture transmission function and the dependence on exposure time and geometrical factors.

We shall consider a pinhole gamma-ray camera forming a projection of a planar object onto the detector plane as the imaging operation. We assume that the pinhole aperture is infinitely thin. For this problem the $\mathbf{H}$ matrix operator reduces to a simple convolution operation.[1] Results will be presented for soft-edged Gaussian apertures as well as hard-edged square apertures. To show explicitly the dependence of the image on exposure time, we rewrite the expression for the mean image of a particular object as shown below:

$$\bar{g}_f(\mathbf{r}) = \kappa h(\mathbf{r}) ** f(\mathbf{r}), \tag{2}$$

where $f(\mathbf{r})$ is the mean number of photons per unit time emitted into all space from an elemental area d^2r located at point $\mathbf{r}$, $h(\mathbf{r})$ is the aperture transmission function, and the

double asterisk denotes a two-dimensional convolution operation. The parameter κ is an efficiency factor that includes the geometry of the imaging system as well as the exposure time T:

$$\kappa = \frac{T}{4\pi(l_1 + l_2)^2}. \tag{3}$$

Here l_1 is the distance from the object to the aperture plane and l_2 is the distance from the aperture to the detector plane. In the matrix notation that we shall use throughout this paper, the parameter κ is implicitly carried by the system operator **H**. By varying κ, we shall assess the dependence of system performance on exposure time, exploring the effect of increasing conspicuity on task performance.

Task Definitions

In general there are two types of task that are of interest when discussing imaging system performance. The first type of task can be termed classification tasks in that the observer's job is to decide the class membership of an object. A physician might face the task of choosing whether the underlying object in a medical image is from the class of patients with disease or the class of normal, nondiseased patients. In astronomy, the classification task might be to decide whether an object is a single star or a binary star. The second type of task consists of those that require a quantitative estimate of some object parameter and are hence termed estimation tasks. An example of an estimation task would be the determination of the activity in some region of interest in the object. In this paper we shall be concerned with simple binary classification tasks for which the detected data are to be used to determine which of two hypotheses is true for the underlying object. Relationships between figures of merit for estimation and classification tasks for objective assessment of image quality are described in a paper in this issue by Barrett.[7]

Our studies are based on two classification tasks: (1) the detection task, for which an observer must determine whether there is a known signal in a known location in the image, and (2) the Rayleigh task, for which the observer must decide whether an image contains a single or a double Gaussian signal. We assume that the object is planar and that the background has infinite spatial extent for both tasks.

Detection Task

In the first study that we shall describe, the signal that is to be detected is a discretized version of the two-dimensional Gaussian function $s(\mathbf{r})$, where $\mathbf{r}$ is the two-dimensional position vector:

$$s(\mathbf{r}) = s(0)\exp(-|\mathbf{r}|^2/2\sigma_s^2). \tag{4}$$

Under the null hypothesis H_1, the signal is absent and the object $f(\mathbf{r})$ is an inhomogeneous (lumpy) background specified by a nonrandom dc level to which is added a random part characterized by a Gaussian spatial autocorrelation function with correlation length σ_B and dc power $W_f(0)$. The mean level $\bar{B}$ is the mean number of photons per unit time emitted into all space from an elemental area of the background and therefore has units of counts per second per area. The average background level is independent of location since the nonuniformity in the background is stationary. (The extension to the more general problem of a uniform background of random level with an added random, spatially varying component is straightforward.) The power spectrum of the random part of the background is written as

$$W_f(\boldsymbol{\rho}) = W_f(0)\exp(-4\pi^2|\boldsymbol{\rho}|^2\sigma_B^2), \tag{5}$$

where $\boldsymbol{\rho}$ is the two-dimensional frequency variable in the Fourier domain conjugate to $\mathbf{r}$. Under hypothesis H_2, the object $f(\mathbf{r})$ is the signal $s(\mathbf{r})$ added to the background described above.

Figure 1 shows four lumpy backgrounds of constant correlation length with increasing values of the power spectrum of the inhomogeneous background at zero frequency $W_f(0)$. Each object contains the same Gaussian signal superimposed upon the lumpy background in the center of the array. The figure also shows sample images of each object after simulating the imaging operation of Eq. (1) with Gaussian apertures of four different sizes. Moving from left to right in the figure shows the effect of increasing aperture size, while moving from top to bottom shows the effect of increasing background inhomogeneity.

Rayleigh Discrimination Task

The second task involves the discrimination between images of single and double Gaussian signals. Under hypothesis H_1 the signal is a single Gaussian of known amplitude $s(0)$ and width σ_s as described in Eq. (4) above. Under hypothesis H_2 the signal is a double Gaussian, for which the amplitude of each Gaussian in the pair is half that of the single Gaussian

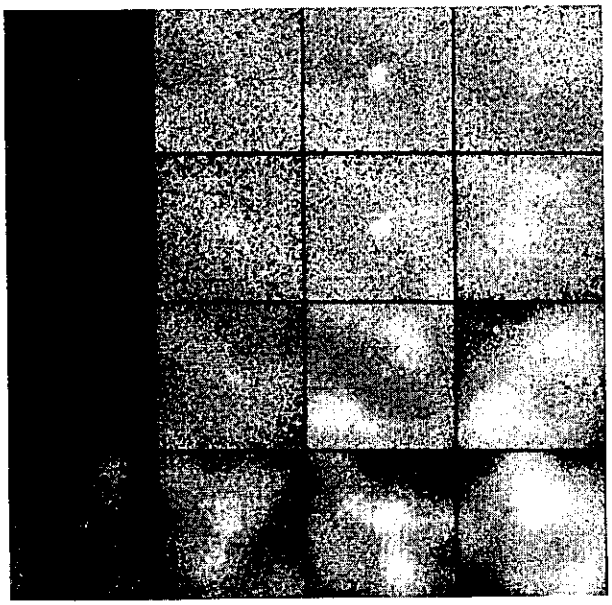

Fig. 1. Illustrative images of a signal on various backgrounds. The left-hand column shows Gaussian-pinhole ($\sigma_p = 0.4\sigma_s$) images of a Gaussian signal (5% contrast, $\sigma_s = 10$ units, centered in the object array) superimposed upon lumpy backgrounds with a correlation length of 30 units for $W_f(0) = 0$, 400, 4000, 40,000 from top to bottom. The second column shows the same objects imaged by a Gaussian aperture with $\sigma_p = 0.8\sigma_s$. The third and fourth columns show the same objects imaged by an aperture size σ_p that is equal to $1.6\sigma_s$ and $3.4\sigma_s$, respectively. The parameters used here are not the same as on the graphs below but rather are chosen to demonstrate detection limitations due to both background inhomogeneity and to Poisson noise.

under H_1, the widths are the same as the width of the single, and the separation and orientation are known. The object under either hypothesis is the appropriate signal added to an inhomogeneous background characterized in the same manner as for the detection task [Eq. (5)].

Signal-to-Noise Ratios and Observers

The ultimate goal of a radiological imaging system often is to provide an image that permits the clinician—a human observer—to make a correct diagnosis. Making accurate measurements of human performance involves psychophysical studies, which are quite tedious and time consuming. There are many circumstances in which we might want to circumvent this lengthy process, such as in the early stages of system optimization. By using models in place of the human observer, we can calculate a figure of merit for an imaging system as a function of many design parameters in a more timely fashion. It is important, though, that the models that we use be predictive of human observer performance when the system is intended for human observers, so that a system optimized for the model observer is optimized for the human as well.

We have already mentioned the Bayesian or ideal observer as a model observer that may be invoked for the assessment of image quality. The literature on signal-detection theory is filled with examples, which are usually taken from radar applications, in which the strategy of the ideal observer is determined for simple detection and discrimination tasks and the associated SNR is calculated.[2,3] The Bayesian approach requires full characterization of the probability-density function of the data under each of the hypotheses. In the literature the signals and backgrounds are often SKE/BKE cases, and the noise is generally assumed to be additive with a Gaussian probability-density function. Then the probability-density function on the data for each hypothesis is Gaussian, and the covariance matrices are equal. The ideal-observer strategy is then easily shown to be the PWMF. The PWMF performs a sequence of linear operations on the data, first undoing any noise correlations that are present and then correlating with a template matched to the expected signal. The optimum test statistic for this SKE/BKE task is therefore a linear function of the data.

If there were no object variability in the present studies, the noise probability law would be Poisson, which might reasonably be approximated by a Gaussian law. If, in addition, the signals to be detected or discriminated are low contrast, the variances on the data are independent of the underlying object. The ideal strategy reduces to the linear PWMF approach in that limit. When the Poisson nature of the data is rigorously included in the ideal-observer SNR calculation, as described in Wagner *et al.*,[5] the ideal strategy remains linear in the data, though not quite the matched filter. Instead, the filter is a logarithmic function of the expected data for each hypothesis.

The presence of the inhomogeneous background in our current studies results in a probability-density function of the data that is potentially not Gaussian. The probability function of the data depends on the entire probability function of the spatially varying component of the background, while only the autocorrelation function of the random background process has been specified. Therefore, the ideal-observer strategy for this problem is not calculable and could involve nonlinear operations on the data. Since there is no evidence that the human observer can perform nonlinear data manipulations,[8] we shall restrict our attention to linear observers for the model observers invoked in the optimization studies presented here.

We define a linear observer as any observer that performs only linear operations on the detected data. We can write the operations of such an observer in matrix form as shown below:

$$\lambda = \mathbf{a}^t\mathbf{g}, \tag{6}$$

where the superscript t denotes the transpose of a vector or matrix. The vector $\mathbf{a}$ represents a template that the observer superimposes upon the data $\mathbf{g}$. The result of this operation is a scalar test statistic λ that is compared with a threshold to permit a decision on which hypothesis is most likely for the given data. Because the test statistic λ is a function of the data, it also has variability due to both the Poisson noise and the inherent object variability.

The SNR of the test statistic λ gives a measure of the separability of the classes. In the literature on signal-detection theory, such a SNR is known as the detectability index d_a and is given by

$$\mathrm{SNR}_\lambda{}^2 = d_a{}^2 = \frac{\Delta\bar{\lambda}^2}{\sigma_\lambda{}^2}, \tag{7}$$

where $\Delta\bar{\lambda}$ is the difference in the means of the test statistic for the two classes and the denominator is the average variance in the test statistic. The variance incorporates both contributions to the randomness in λ, the randomness due to the lumpy background in the object and the Poisson nature of the detected data. This is a meaningful figure of merit as long as the statistics on λ are approximately Gaussian, which is the case here since we see from Eq. (6) that λ is the sum of a large number of random variables and therefore the central-limit theorem may be invoked.

In the next sections we describe the two model observers that we have chosen to investigate and give the prescriptions for their test statistics and associated SNR's.

Hotelling Observer

The Hotelling observer demonstrates maximum discrimination ability among all observers that are limited to performing only linear operations on the data. We designate this observer by the name Hotelling observer because the optimum linear classifier was first presented in a classic paper by Hotelling.[9] We shall describe the Hotelling approach for the two-class (binary) problem relevant for our studies. The generalization to more than two classes can be found in texts on statistical pattern recognition such as that by Fukunaga.[10] The two-class Hotelling approach was previously described for the specific problem of image assessment in medical imaging by Barrett *et al.*[11–13] Fiete *et al.*[14] have shown that the performance of the Hotelling observer and the human observer have high correlation for discrimination tasks that include signal variability.

General Hotelling Theory The Hotelling approach is based on two scatter matrices, $\mathbf{S}_1$ and $\mathbf{S}_2$. These scatter matrices completely describe the first- and second-order statistics of the two classes, where the two classes designate the two possible states of truth regarding the underlying objects: signal present and signal absent in the detection

problem and one source versus two sources for the Rayleigh task. Our discussion above pointed out that the optimum (Bayesian) test statistic is a linear function of the data for the SKE/BKE discrimination problem when the probability-density function of the data under each hypothesis is Gaussian and the covariance matrices are equal. The Hotelling observer reduces any decision problem to a linear test by approximating the probability density functions of the data for each of the classes by Gaussians, each with covariance matrix equal to the average covariance matrix for the two classes. Hence, if the lumpy background were such that the probability-density function on the data were Gaussian with equal covariance matrix for the two hypotheses, the Hotelling or best-linear strategy would be the ideal strategy. However, many other non-Gaussian probability-density functions of the data are consistent with the given information regarding the background. In those non-Gaussian cases the data would have higher-order moments that would not be utilized by the Hotelling observer. The ideal observer would make use of those higher-order moments and would most likely be nonlinear. Methods for simulating lumpy backgrounds with the specified Gaussian autocorrelation function have been described by Rolland.[15]

The interclass scatter matrix $\mathbf{S}_1$, a measure of the distance between the class means, is defined in the two-class problem as follows:

$$\mathbf{S}_1 = \sum_{k=1}^{2} P_k[\langle \mathbf{g} \rangle_k - \langle \mathbf{g} \rangle_0][\langle \mathbf{g} \rangle_k - \langle \mathbf{g} \rangle_0]^t, \tag{8}$$

where P_k is the *a priori* probability of occurrence of class k, $\langle \mathbf{g} \rangle_k$ is the mean data vector for the kth class, and $\langle \mathbf{g} \rangle_0$ is the grand mean of all data vectors in both classes:

$$\langle \mathbf{g} \rangle_0 = P_1 \langle \mathbf{g} \rangle_1 + P_2 \langle \mathbf{g} \rangle_2. \tag{9}$$

If we substitute the definition of the grand mean [Eq. (9)] into Eq. (8), we find that

$$\mathbf{S}_1 = P_1 P_2[\langle \mathbf{g} \rangle_2 - \langle \mathbf{g} \rangle_1][\langle \mathbf{g} \rangle_2 - \langle \mathbf{g} \rangle_1]^t \tag{10}$$

in the two-class problem.

The intraclass scatter matrix $\mathbf{S}_2$ is the average covariance matrix of the classes:

$$\mathbf{S}_2 = P_1 \mathbf{C}_1 + P_2 \mathbf{C}_2, \tag{11}$$

where $\mathbf{C}_1$ and $\mathbf{C}_2$ are the covariance matrices for classes 1 and 2, respectively. The covariance matrix of the kth class is defined as

$$\mathbf{C}_k = \langle [\mathbf{g} - \langle \mathbf{g} \rangle_k][\mathbf{g} - \langle \mathbf{g} \rangle_k]^t \rangle. \tag{12}$$

The beauty of the Hotelling formalism is that the optimum linear filter and the figure of merit for the Hotelling observer are fully specified once the scatter matrices $\mathbf{S}_1$ and $\mathbf{S}_2$ are determined. Previous authors have reported on the method for deriving the optimum linear filter through an eigenvector analysis of the product $\mathbf{S}_2^{-1}\mathbf{S}_1$.[13,16] The Hotelling test statistic can be shown to be

$$\begin{aligned} \lambda_{\text{Hot}} &= [\langle \mathbf{g} \rangle_2 - \langle \mathbf{g} \rangle_1]^t \mathbf{S}_2^{-1} \mathbf{g} \\ &= \mathbf{a}_{\text{Hot}}^t \mathbf{g}. \end{aligned} \tag{13}$$

This is a generalization of the PWMF. The presence of $\mathbf{S}_2^{-1}$ in the expression means that the Hotelling observer attempts to compensate for object variability in addition to the prewhitening of noise correlations performed by the PWMF. When there is no object variability, $\mathbf{S}_2$ represents only noise correlations in the data, and the Hotelling observer reduces to the PWMF.

The Hotelling trace criterion (HTC) is a scalar figure of merit for the Hotelling observer. It is known in the literature as J or HTC and is defined in terms of the scatter matrices as

$$J = \text{tr}[\mathbf{S}_2^{-1}\mathbf{S}_1], \tag{14}$$

where tr denotes the trace of a matrix. The HTC is an intuitively appealing measure of class separability because we see from Eq. (14) that it increases with increased interclass separation ($\mathbf{S}_1$) and decreases with increased class variance ($\mathbf{S}_2$). The HTC is related to the SNR of the test statistic λ_{Hot} by

$$J = P_1 P_2 \text{SNR}_{\text{Hot}}^2. \tag{15}$$

Thus J is a generalization of the detectability index d_a of signal-detection theory.

In the next section we use the general expressions presented here to derive the SNR of the Hotelling observer for the discrimination problem in the presence of a lumpy background.

Hotelling Approach to Lumpy Background Problem To determine a figure of merit for the Hotelling observer, we must first determine the first- and second-order statistics on the data that lead to the scatter matrices $\mathbf{S}_1$ and $\mathbf{S}_2$. For a particular object $\mathbf{f}$, the detected data are conditionally Poisson, with the mean given by

$$\bar{\mathbf{g}}_f = \langle \mathbf{g} \rangle_{n|f}. \tag{16}$$

The angle brackets and associated subscript denote an average over the Poisson noise in the image for a given realization of the object. To find the mean image given that hypothesis $H_k (k = 1, 2)$ is true, we average the conditional mean over all objects that belong to class k:

$$\begin{aligned} \bar{\mathbf{g}}_k &= \langle \mathbf{g} \rangle_k \\ &= \langle \bar{\mathbf{g}}_f \rangle_{f|k} \\ &= \langle \langle \mathbf{g} \rangle_{n|f} \rangle_{f|k}, \end{aligned} \tag{17}$$

where the outer average is over the ensemble of all objects in the kth class. If the two classes are equally likely, the interclass scatter matrix [Eq. (10)] is given by

$$\begin{aligned} \mathbf{S}_1 &= \tfrac{1}{4}(\bar{\mathbf{g}}_2 - \bar{\mathbf{g}}_1)(\bar{\mathbf{g}}_2 - \bar{\mathbf{g}}_1)^t \\ &= \tfrac{1}{4}(\Delta \bar{\mathbf{g}})(\Delta \bar{\mathbf{g}})^t. \end{aligned} \tag{18}$$

Since the background has equivalent statistics under each hypothesis and since the signal is nonrandom, the difference in overall class means that $\Delta \bar{\mathbf{g}}$ is simply the image of the difference signal:

$$\Delta \bar{\mathbf{g}} = \mathbf{H}(\bar{\mathbf{f}}_2 - \bar{\mathbf{f}}_1) = \mathbf{H}\Delta \mathbf{s}, \tag{19}$$

so that

$$\mathbf{S}_1 = \tfrac{1}{4}(\mathbf{H}\Delta \mathbf{s})(\mathbf{H}\Delta \mathbf{s})^t. \tag{20}$$

The covariance matrix of the kth class is defined as

$$\mathbf{C}_k = \langle\langle(\mathbf{g} - \bar{\mathbf{g}}_k)(\mathbf{g} - \bar{\mathbf{g}}_k)^t\rangle_{n|f}\rangle_{f|k}. \tag{21}$$

Since the object inhomogeneity is the same under both classes, the covariance matrices are approximately equal in the low-contrast limit ($\mathbf{C}_1 \simeq \mathbf{C}_2 \simeq \mathbf{C}$). Thus, for our low-contrast SKE problem, we see from Eq. (11) that $\mathbf{S}_2$ is simply equal to $\mathbf{C}$. Appendix A gives the derivation of the covariance matrix $\mathbf{C}$. We find the value in the ith row and the jth column to be

$$S_2(i, j) = C(i, j) = R_g(i, j) + \kappa A_{ap}\bar{B}\delta_{ij}, \tag{22}$$

where $\mathbf{R}_g$ is the autocorrelation of the data due to the nonuniform background and A_{ap} is the area of the aperture. We see that the covariance matrix is a sum of two matrices, one containing the randomness of the object that is due to the lumpy background $\mathbf{R}_g$ and the other a diagonal matrix containing the variance associated with the Poisson nature of the detected data.

If we substitute the expressions for the scatter matrices into the equation for the Hotelling test statistic [Eq. (13)], we find that

$$\begin{aligned}\lambda_{Hot} &= [\langle\mathbf{g}\rangle_2 - \langle\mathbf{g}\rangle_1]^t\mathbf{S}_2^{-1}\mathbf{g} \\ &= \Delta\mathbf{g}^t S_2^{-1}\mathbf{g} \\ &= (\mathbf{H}\Delta\mathbf{s})^t\mathbf{C}^{-1}\mathbf{g}.\end{aligned} \tag{23}$$

If we substitute the same expressions for the scatter matrices into Eqs. (14) and (15), for equal-probability classes, we find the Hotelling observer's SNR to be

$$\begin{aligned}\mathrm{SNR}_{Hot}^2 &= 4\mathbf{J} \\ &= 4\ \mathrm{tr}[\mathbf{S}_2^{-1}\mathbf{S}_1] \\ &= \mathrm{tr}[\mathbf{C}^{-1}(\mathbf{H}\Delta\mathbf{s})(\mathbf{H}\Delta\mathbf{s})^t] \\ &= \Delta\mathbf{s}^t\mathbf{H}^t\mathbf{C}^{-1}\mathbf{H}\Delta\mathbf{s}.\end{aligned} \tag{24}$$

The full expression for the Hotelling observer's SNR for linear, shift-invariant systems and stationary statistics is derived in Appendix B and given as an integral over the Fourier domain below:

$$\mathrm{SNR}_{Hot}^2 = \int_\infty d^2\rho\, \frac{|\Delta\tilde{s}(\rho)|^2|\tilde{H}(\rho)|^2}{[\kappa A_{ap}\bar{B} + |\tilde{H}(\rho)|^2 W_f(\rho)]}, \tag{25}$$

where a tilde above a function signifies its Fourier transform. Thus $\tilde{H}(\rho)$ is the system transfer function and $\Delta\tilde{s}(\rho)$ is the Fourier transform of the difference signal $\Delta s(\mathbf{r})$.

The integrand in Eq. (25) may be identified in terms of a generalization of the frequency-dependent noise-equivalent quanta (NEQ) for the lumpy-background discrimination problem.[17] The NEQ concept was introduced by Shaw[18,19] and has been used extensively by Wagner[20] and others for SKE discrimination tasks. The generalized NEQ are given by

$$\mathrm{NEQ}(\rho) = \frac{|\tilde{H}(\rho)|^2}{[\kappa A_{ap}\bar{B} + |\tilde{H}(\rho)|^2 W_f(\rho)]}. \tag{26}$$

Equation (25) will have units appropriate to NEQ when it is normalized such that the difference signal is written as a contrast with respect to the background. The usual expression for NEQ(ρ) for the flat-background problem is recovered from this form by setting $W_f(\rho)$ equal to zero and recognizing that $\kappa A_{ap}\bar{B}$ is the Poisson noise power spectral density for that case.

Nonprewhitening Matched Filter

The second model observer that we shall consider is the nonprewhitening matched filter (NPWMF). The NPWMF strategy is to apply a simple template matched to the expected difference signal to form a test statistic:

$$\lambda_{npw} = (\mathbf{H}\Delta\mathbf{s})^t\mathbf{g}. \tag{27}$$

The NPWMF test statistic λ_{npw} is a linear function of the data $\mathbf{g}$. Any correlations in the noise or spatial variations in the background are not corrected for by this observer. Our interest in this observer comes from the fact that, in studies of human detection and discrimination performance for SKE/BKE tasks with correlated noise, this observer has been found to be a good predictor of human performance.[21,22]

We again use the definition of observer SNR of Eq. (7) to derive the figure of merit for the NPWMF. Although the NPWMF observer takes no account of the statistics of either the Poisson noise or the background fluctuations, these statistics are included in the statistics of λ_{npw} when the averages in Eq. (7) are performed. Appendix C derives SNR_{npw} and shows its Fourier representation to be equal to

$$\mathrm{SNR}_{npw}^2 = \frac{\left[\int_\infty d^2\rho|\Delta\tilde{s}(\rho)|^2|\tilde{H}(\rho)|^2\right]^2}{\int_\infty d^2\rho|\Delta\tilde{s}(\rho)|^2|\tilde{H}(\rho)|^2\kappa A_{ap}\bar{B} + \int_\infty d^2\rho|\Delta\tilde{s}(\rho)|^2|\tilde{H}(\rho)|^4 W_f(\rho)}. \tag{28}$$

It is straightforward to relate both the numerator and the denominator of Eq. (28) to the scatter matrices used in the Hotelling approach.[7] The numerator of Eq. (28) is the squared integral of the energy of the difference signal in the frequency domain. As can be seen from Eq. (20), the trace of the interclass scatter matrix is an equivalent representation of the sum of the energy of the difference signal for the discretized signal in the spatial domain. The denominator of Eq. (28) is the integral of the difference signal energy multiplied by the power spectrum of the data. In the spatial-domain matrix notation the denominator should therefore be expected to contain the product of the interclass scatter matrix $\mathbf{S}_1$ and the intraclass scatter matrix $\mathbf{S}_2$. The actual result is given below:

$$\mathrm{SNR}_{npw}^2 = \frac{\mathrm{tr}[\mathbf{S}_1]^2}{\mathrm{tr}[\mathbf{S}_1\mathbf{S}_2]}. \tag{29}$$

The frequency-domain expression of Eq. (28) is valid only in the low-contrast limit where stationary statistics apply. At high contrasts the Poisson contribution to the variance in the data is nonstationary, so that the Fourier transform of the covariance matrix of the data is no longer diagonal. The expression for the variance is still the sum of two terms, one representing the Poisson variance and the other representing the variation in the background, as shown in Appendix C, Eq. (C9). In this work high-contrast SNR_{npw} results were

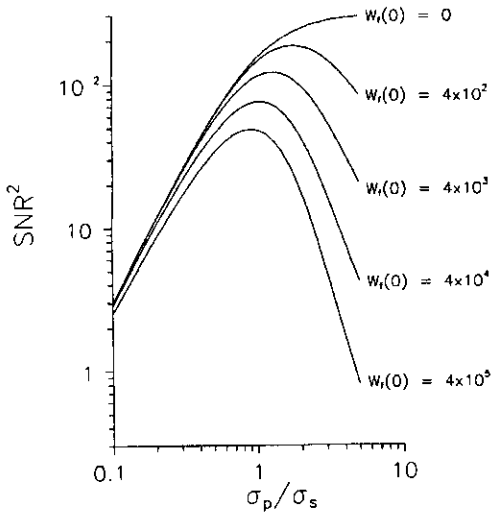

Fig. 2. Family of Hotelling SNR^2 curves as a function of the ratio of the Gaussian aperture width to the signal width for a detection task. The plots show the effect of increasing the value of the power spectral density of the background at zero spatial frequency, $W_f(0)$. The signal width is 10 units, and the width of the autocorrelation function of the background is 30 units. The signal contrast is 5%.

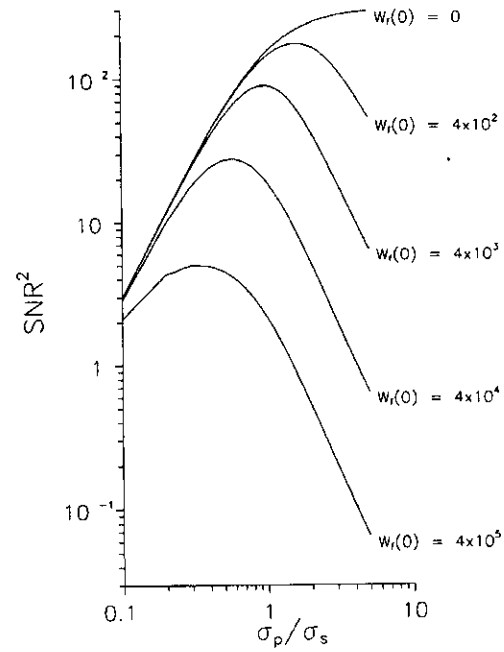

Fig. 3. Plot of the NPWMF SNR^2 as a function of the Gaussian aperture width to the signal width for the same detection task as in Fig. 2.

calculated through space-domain computations of the means and Poisson variances of the data by using convolutions. A similar space-domain approach was presented by Wagner *et al.*[5] for the high-contrast SKE/BKE Rayleigh task, although the template in that paper was the PWMF for the Poisson-noise case (logarithmic in the expected difference signal). In the inhomogeneous-background problem here, the approach of Wagner *et al.* must also be modified to permit the addition to the SNR denominator of the variance that is due to the lumpy background. Since the lumpy background is stationary and independent of the signal amplitude, its contribution to the variance can still be calculated in the Fourier domain just as it was in the low-contrast case.

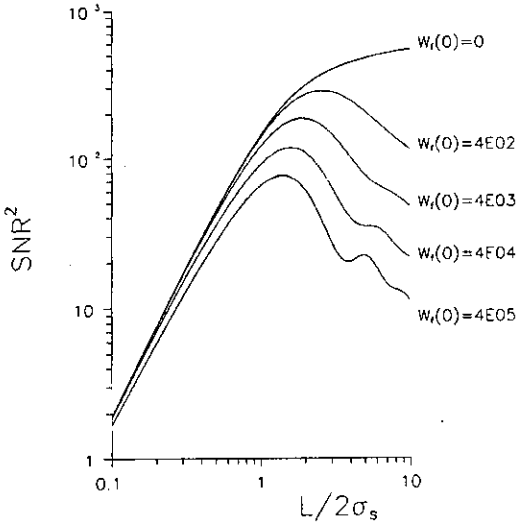

Fig. 4. Plot of the Hotelling SNR^2 for the detection task with a square aperture of length L on a side. The abscissa is the ratio of the square aperture length to the signal width. The signal width is 10 units, and the width of the autocorrelation function of the background is 30 units. The signal contrast is 5%.

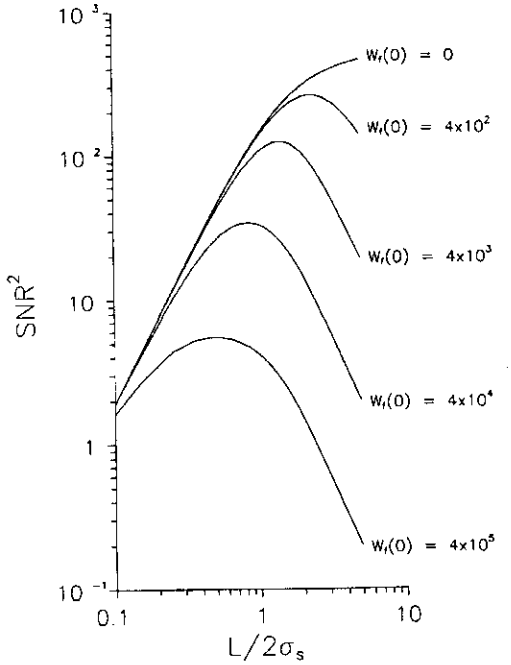

Fig. 5. Plot of the NPWMF SNR^2 as a function of the ratio of the side length of the square aperture to the signal width. The signal and background parameters are the same as for Fig. 4.

RESULTS

In order to calculate the SNR's of Eqs. (25) and (28), we must first choose reasonable values for the signal parameters and imaging system factors. For all the low-contrast results that we shall present, the Gaussian signals had a width σ_s of 10 mm. The correlation length of the lumpy background in all low-contrast cases was set equal to 30 mm, so that $\sigma_B = 3\sigma_s$. The contrast of the signal with respect to the mean background level $\bar{B}$ was 5%. This contrast value is a realistic, albeit challenging, value for nuclear-medicine applications. To achieve this contrast figure, we set the background level $\bar{B}$ equal to 610 counts/(sec-mm^2), which then sets the signal amplitude $s(0)$. The background level $\bar{B}$ was chosen to imply 10^7 disintegrations in the given imaging time in a 128 mm × 128 mm object, so that one could detect 10^7 counts in a perfect collection system. For all studies in which the exposure time T was not a variable, κ was a constant set equal to 0.001 sec/mm^2.

Detection Task

Figure 2 is a plot of SNR_{Hot} for the low-contrast detection task as a function of Gaussian aperture diameter σ_p for increasing levels of the background parameter $W_f(0)$. Figure 3 is a similar plot for the NPWMF. The upper curve in both figures corresponds to a uniform background, for which both observers reduce to the ideal observer. These curves were derived through numerical integration of Eqs. (25) and (28) for Figs. 2 and 3, respectively. Note that in the uniform-background case, in which the observer performance is purely quantum limited, the aperture should be as large as possible to collect as many photons as possible. This result is consistent with the finding of Tsui *et al.*[4]

In the presence of a lumpy background the SNR's of both observers demonstrate a clear optimum size. We have normalized the abscissa by the signal size σ_s in all figures to clarify the relationship between the optimum aperture size and the size of the signal. For all values of $W_f(0)$ we find that the optimum aperture size is generally the same size as the signal. The NPWMF is seen to experience a greater performance penalty than the Hotelling observer as the aperture size is increased beyond the optimum value.

Figures 4 and 5 repeat the calculations of Figs. 2 and 3, replacing the Gaussian aperture with a square aperture of area L^2. Little difference between the Gaussian aperture and square aperture for the NPWMF can be observed. However, there is a marked difference in the performance of the Hotelling observer for the square aperture, for we now find oscillations in the SNR_{Hot} graph. Some intuition regarding the presence of these oscillations can be obtained from a frequency-domain point of view, where the Fourier transform of the square aperture becomes an oscillatory function in the integral of Eq. (25). As the square size L increases, its sinc function in the Fourier picture narrows, and oscillatory lobes in the transfer function move toward zero frequency. Certain ranges of L beyond the optimum size evidently result in particular positions of the maxima and minima of the sinc that result in local improvements in the discriminability between signal and background, resulting in small oscillations in SNR_{Hot}.

Figure 6 gives a family of curves for the NPWMF performing a high-contrast detection task. The signal amplitude in this case was 1000 times the mean background level. For this task the signal width was 5 pixels or 5 mm and the background correlation length was 15 units or 15 pixels, so that, again, $\sigma_B = 3\sigma_s$. (We reduced the size of the signal in this case to ease the array size requirements on the space-domain convolutions required to calculate the SNR for the largest apertures.) We have found in general that the high-contrast results are similar to the low-contrast results with the magnitudes of the SNR's increased. The spatially varying background limits the performance of the observer in the same way, and the optimum aperture size remains more or less the same. The similar character of the high- and low-contrast SNR_{npw} curves indicates that the signal-to-mean-background contrast is not by itself an important parameter in the lumpy-background problem, at least for this model observer. Instead, the ratio of the contrast to the background parameter $W_f(0)$ must be taken into consideration.

A striking difference between the Hotelling observer and the NPWMF observer is found by plotting the detection performance of each as a function of exposure time T (effected by increasing κ). These plots are given in Figs. 7 and 8 for increasing values of the background spectral density level $W_f(0)$. When $W_f(0)$ is zero, the background is uniform, and both observers reduce to the ideal observer, whose performance increases linearly with exposure time. Figure 7 shows a power-law increase in SNR_{Hot} as a function of T for all nonzero values of $W_f(0)$, with the slope approximately equal to 2/3. No evidence of saturation of the Hotelling observer performance can be observed in the plot. Figure 8 demonstrates a hard saturation in the performance of the NPWMF for the same set of tasks. The behavior of the NPWMF is predicted from the expression for the SNR_{npw} given in Eq. (28). Since each system operator (and its Fourier trans-

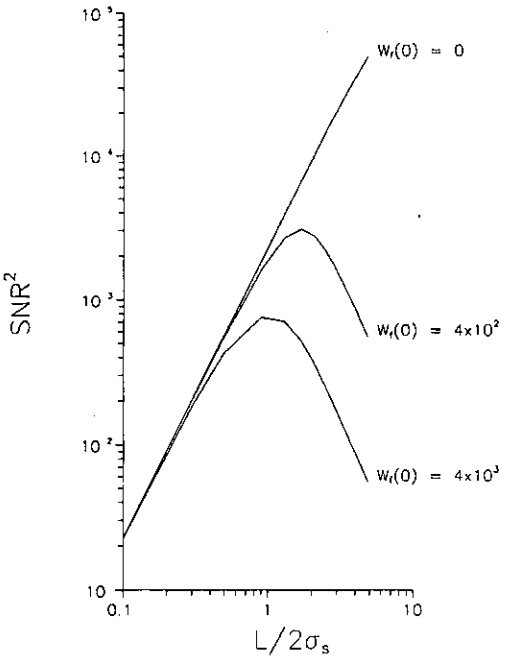

Fig. 6. NPWMF SNR^2 for a high-contrast detection task. The signal strength is 10 times the background, the signal width is 5 units, and the background autocorrelation length is 15 units.

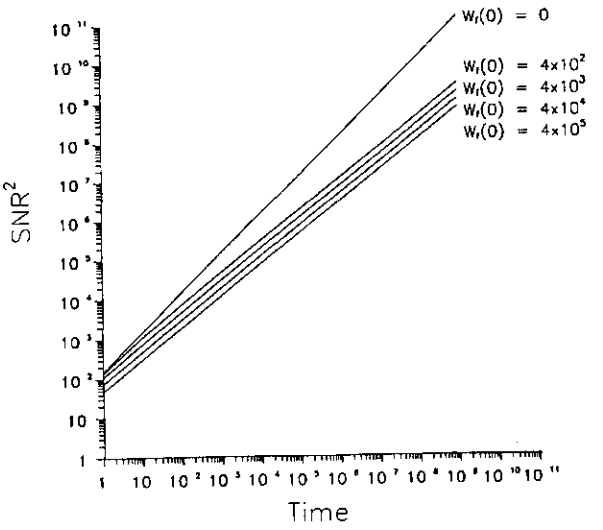

Fig. 7. Hotelling SNR^2 as a function of exposure time for a detection task. The signal width is 10 units, and the background autocorrelation length is 30 units. The Gaussian aperture width is equal to the signal width, and the signal contrast is 5%.

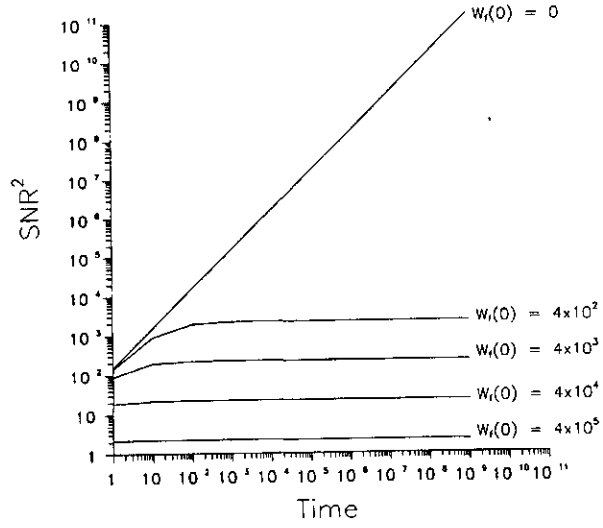

Fig. 8. NPWMF SNR^2 versus exposure time for the same detection task as in Fig. 7.

form) carries along the time-dependence parameter κ, the numerator in the $\mathrm{SNR}^2_{\mathrm{npw}}$ and the background variance term are both proportional to κ^4 or T^4, while the Poisson variance term is proportional to κ^3 or T^3. This leads to

$$\mathrm{SNR}^2_{\mathrm{npw}} \propto \frac{\alpha T^4}{\beta T^3 + \gamma T^4}. \tag{30}$$

As T becomes large, $\mathrm{SNR}_{\mathrm{npw}}{}^2$ goes to a constant for any aperture size. Since the magnitude of the γT^4 term is much larger for a large aperture (it goes as L^8), the conspicuity limit sets in earlier for larger apertures.

It is difficult to get the same kind of intuition regarding the time dependence of the Hotelling SNR because the numerator and the denominator in the $\mathrm{SNR}_{\mathrm{Hot}}$ expression are interacting within the same integral. (This is also true when one is trying to investigate the behavior of the Hotelling SNR for large aperture size L.) Instead we can look to the space- and Fourier-domain pictures of the Hotelling template (Figs. 9 and 10) for insight regarding the Hotelling result. Figure 9 is a one-dimensional schematic of the Hotelling template $\mathbf{a}_{\mathrm{Hot}} = \mathbf{C}^{-1}\mathbf{H}\Delta\mathbf{s}$ in the space domain for the lumpy-background detection problem with a Gaussian aperture (the two-dimensional function is rotationally symmetric for this aperture), and Fig. 10 gives the Fourier-domain filter function. We see from Fig. 9 that the Hotelling observer's strategy in the detection problem, in effect, is to use the area surrounding the known signal location to get an estimate of the local background level. The observer subtracts this background estimate from a measure of the counts in the signal region to determine whether the count density in the signal location is high enough to be called "signal present." This differencing operation in the space domain is equivalent to a high-pass filter in the frequency domain, as seen in Fig. 10. As long as the background autocorrelation function has a length that is different from the signal size, the Hotelling observer can look in the Fourier domain for the signal in the frequency channels where the signal and the background differ significantly. For these studies, the signal width σ_s is 1/3 the background correlation length σ_B. The signal spectrum is therefore wider than the spectrum of the background. The Hotelling observer makes use of this information by making the discrimination based on measuring the amount of power in the higher frequencies. As the

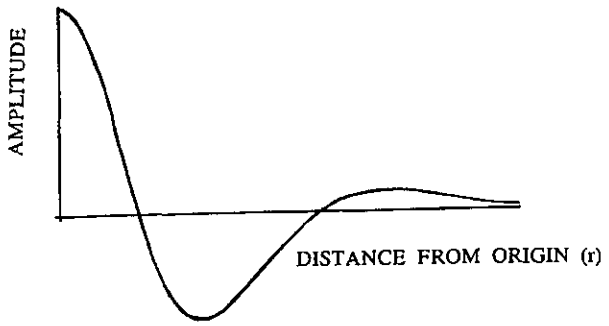

Fig. 9. Schematic of the Hotelling template along a radial axis in the space domain for the detection of a Gaussian object on a lumpy background imaged through a Gaussian aperture.

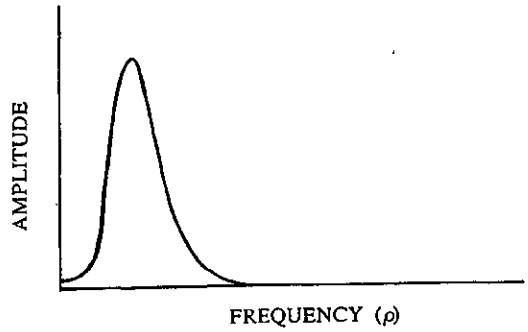

Fig. 10. Schematic of the Fourier filter corresponding to the Hotelling template for the detection of a Gaussian object on a lumpy background imaged through a Gaussian aperture.

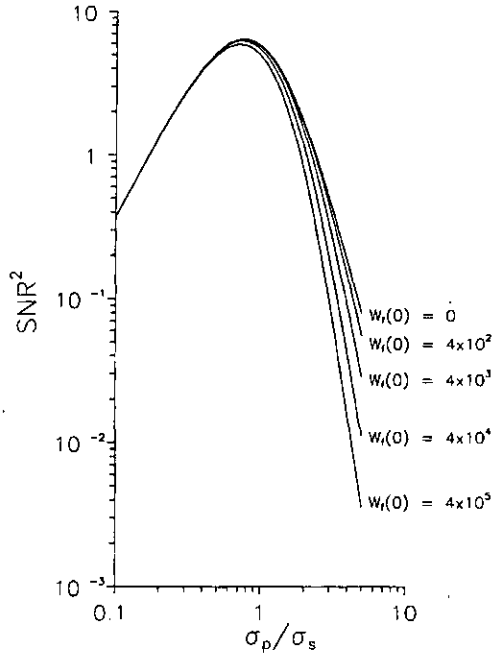

Fig. 11. Plot of the Hotelling SNR^2 for the Rayleigh discrimination task for Gaussian apertures of varying size σ_p. The source width is 10 units, and the pair separation is 20 units. The contrast and background parameters are the same as in Fig. 2.

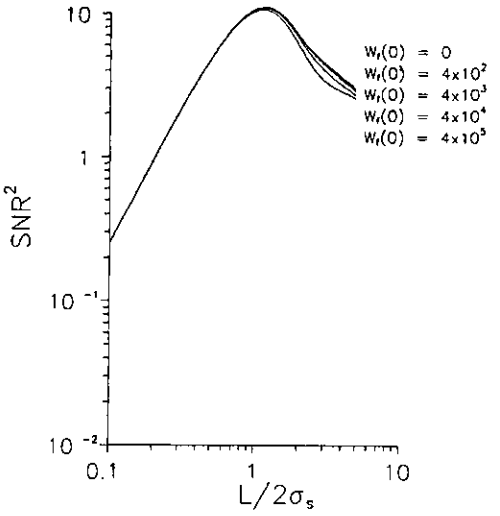

Fig. 12. Plot of the Hotelling SNR^2 for the Rayleigh discrimination task for square apertures of varying length L on a side. The source width is 10 units, and the pair separation is 30 units. The contrast and background parameters are the same as in Fig. 2.

exposure time increases, the quality of information in the higher frequencies of the data improves. Unlike the NPWMF, the Hotelling strategy is different for each exposure time since the Hotelling template depends on the variance in the data. Because the Hotelling observer adjusts its template as the higher-frequency information improves with higher exposure times, the Hotelling performance never saturates. On the other hand, the NPWMF uses the same simple template matched to the difference signal for all exposure times. Even though increasing the exposure time reduces the quantum fluctuations in the data, the observer is limited by an inability to compensate for the varying background. Thus the NPWMF becomes conspicuity limited in the limit of large exposure times.

Rayleigh Discrimination Task

Figures 11 and 12 exhibit representative results for the Hotelling observer for the Rayleigh discrimination task for Gaussian and for square apertures, respectively. In this case the optimum aperture size is comparable with the size

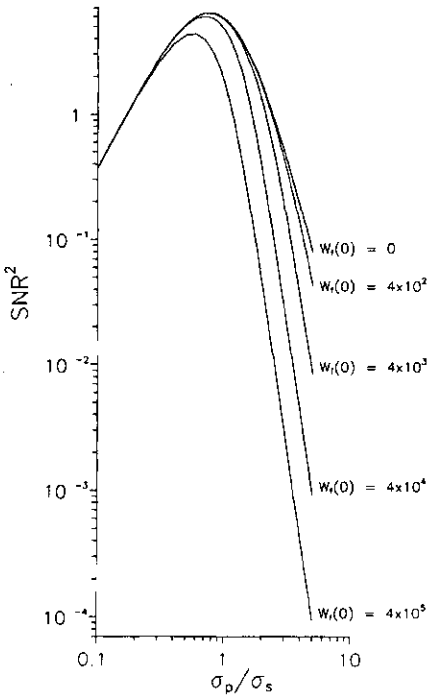

Fig. 13. Plot of the NPWMF observer SNR^2 for the Rayleigh resolution task with a Gaussian aperture, as described in Fig. 11.

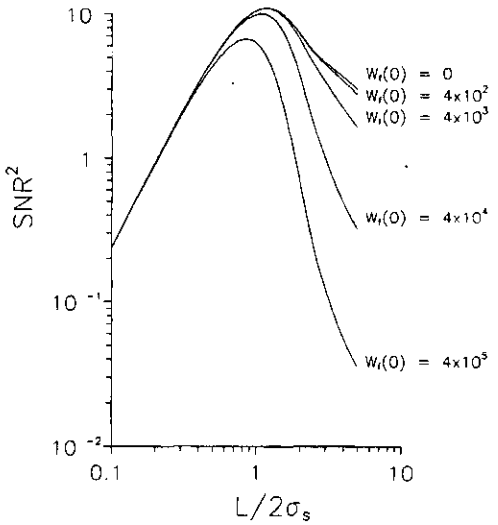

Fig. 14. Plot of the NPWMF observer SNR^2 for the Rayleigh resolution task with a square aperture as described in Fig. 12.

of the signal even without background inhomogeneity. The figures show that only a small performance degradation occurs for the Hotelling observer when a lumpy background is introduced for Gaussian and for square apertures. The differencing operation performed by the Hotelling observer is quite effective at distinguishing background from signal for this task, partly because the double signal does not effectively mimic the symmetry of the background lumps. We see some evidence of oscillations in the curves for the square aperture and the Hotelling observer, again because of the effect of an oscillatory function in the Fourier-domain integral.

Finally, Figs. 13 and 14 show the Rayleigh discrimination ability of the NPWMF for Gaussian and square apertures, respectively. We see that the large apertures are much more strongly affected by the presence of the lumpy background than the smaller ones, regardless of aperture shape.

DISCUSSION

In all cases that we have considered, plots of SNR^2 versus aperture size have an initial slope equal to 2. This is the regime of negligible blur, so that the counts collected from the signal region just go up with the aperture area. When the aperture size becomes appreciable, the image is blurred by convolution with the aperture, spreading the signal counts out over a larger region of the detector plane, and SNR^2 either saturates or goes through a maximum, depending on the observer and the background lumpiness. Without lumpiness [$W_f(0) = 0$], the Hotelling and NPWMF observers both reduce to the ideal observer, which is a matched filter that knows where to look for the signal counts that are spread out by the aperture and gather them all up again. Thus, with sizable blur, the counts from the signal region on the detector plane collected by the observer still grow with aperture area (L^2). In the uniform-background case, the area of the background that contributes at any one detector element continues to grow as L^2 as the aperture size increases (because we have assumed a background of infinite spatial extent). Since the area over which the ideal observer has to look for a signal increases by L^2, the background that contributes to the noise in the ideal-observer test statistic grows as L^4, and the standard deviation increases as L^2. The performance of the ideal observer therefore saturates. While the optimum aperture size in the flat-background case is infinite, the ideal-observer SNR^2 asymptotically approaches $c^2\kappa\bar{B}(A_s^2/2)$, where c is the contrast [$c = s(0)/\bar{B}$] and A_s is the area of the signal (e.g., Gaussian signal area = $2\pi\sigma_s^2$).

If a spatially varying component is then added to the flat background, the slope at large aperture dimensions for the detection problem decreases further for both the Hotelling and the NPWMF observers. Larger apertures collect more of the lumpy background into each detector element, and this extra variation effectively increases the noise in the observer's test statistic. We have seen, though, that the Hotelling observer can cope with the lumpiness to a much greater extent by a local background-correction scheme. We would expect this correction scheme to falter as the background-correlation length approaches the size of the signal.

The template used by the ideal observer when the background is uniform is simply the image of the difference signal $\mathbf{H}\Delta\mathbf{s}$. In the detection task, the template is therefore just the image of the Gaussian signal itself. In the Rayleigh task, the template for the uniform-background case is the image of the double Gaussian subtracted from the image of the single Gaussian, resulting in a template that looks much like the one that is shown in Fig. 10 for the Hotelling observer for detection in the presence of a lumpy background. Thus the simple differencing operation performed by the Hotelling observer for a flat background in the Rayleigh task results in a template that closely resembles the detection template of the Hotelling observer with a lumpy background. The Hotelling observer uses a high-frequency filter to perform both tasks. The filters for the two problems differ slightly in that the flat-background Rayleigh task yields a frequency-domain filter that is zero at $\rho = 0$ (because the mean number of counts in the image gives no discrimination), while the lumpy-background detection task has a small but nonzero frequency-domain-filter value at zero spatial frequency to attempt to discriminate on the basis of the signal energy.

In the Rayleigh task at low contrast, the optimum aperture size is comparable with the size of the signal even without background inhomogeneity. Larger apertures strongly degrade performance in the flat-background case. When the background is spatially varying the NPWMF pays an even larger performance penalty for aperture sizes beyond the optimum, while the Hotelling observer is affected only slightly. Myers *et al.*[23] have reported that, at high contrasts, the performance of the ideal observer in the flat-background Rayleigh task apparently does not saturate with increasing aperture size. More investigations into the transition from the low- to high-contrast regime are needed to explain this further and to determine the effect of background nonuniformity on aperture choice for the high-contrast Rayleigh task.

For low-contrast tasks, interpretations in the frequency domain are valid and can give good insight, as we have seen particularly in understanding the strategy of the Hotelling observer. Caution must be exercised in attempting to extend this insight to the high-contrast limit, for which the frequency-domain picture is not appropriate. At high contrasts a space-domain calculation must be employed, owing to the nonstationary nature of the covariance matrices and the correlations between Fourier components that result.

A remaining question is the relationship between these results and the discrimination ability of the human observer for the same tasks. Tasks that lead to strikingly different results for the Hotelling and the NPWMF observers, such as the exposure-time study, permit us to test to see which observer model is a better predictor of human performance for that task. Results of psychophysical studies of human performance on the same tasks as those investigated here will be presented in a future publication by Rolland.[15]

This work also has implications for machine readers, that is, computer algorithms designed to do classification tasks. In cases for which there is a great difference in performance between the two model observers, simple nonprewhitening templates should be avoided. Instead, automated algorithms should be designed to incorporate statistics of the background whenever possible. The Hotelling framework provides a straightforward method for calculating the best linear template for performing discrimination tasks in a varying background.

While this paper has considered only simple open aper-

tures of varying size, low-contrast performance of other apertures could equally well have been investigated by using their appropriate Fourier expressions in Eqs. (25) and (28). More complicated apertures, such as coded apertures, for example, could therefore be assessed on the basis of model-observer task performance and compared with the simple open apertures for the lumpy-background case. Similarly, performance assessment based on other SKE tasks (sine-wave detection, etc.) can be easily achieved through appropriate manipulation of the difference-signal term in the expressions for the SNR's. High-contrast comparisons for other apertures or for different discrimination tasks could be done just as high-contrast results were presented here. The calculations are not so pretty: part of the calculation must be done by using lengthy convolutions in the space domain.

These studies evaluated the ability of model observers to perform simple detection and discrimination tasks. While these studies have included a spatially varying background, further investigations are needed to determine the ability of the model observers to perform still more complex tasks, including tasks for which there is uncertainty in signal parameters such as size, amplitude, and location, to simulate further more realistic tasks. Also, all performance measures derived in this work were based on using the raw data to perform the appropriate task. It is not clear that humans would be able to use raw data effectively for complicated tasks, so studies comparing model performance on raw and reconstructed data versus human performance on both raw and reconstructed data sets are also warranted. Image assessment based on model observer performance using simulated reconstructions for a variety of tasks is presented in a paper in this issue by Hanson.[24]

While the present studies are based on simulated objects, this research has implications for phantom design as well. We expect that some systems that perform well on stylized phantoms for which the background is known to be flat might demonstrate marked performance degradations with more realistic objects that have spatially varying backgrounds.

CONCLUSION

This work is an extension of the realm of signal-detection theory from the SKE/BKE paradigm into the more realistic situation in which the background is inhomogeneous and specified only statistically. In allowing for a spatially varying background, we have gained new insight into the problem of system optimization in emission imaging in the presence of both quantum limitations and conspicuity limitations.

The present study is interesting in that relatively little numerical computation is needed to derive the low-contrast results. The scatter matrices $\mathbf{S}_1$ and $\mathbf{S}_2$ can be derived analytically, and $\mathbf{S}_2$ can be analytically inverted in the Fourier domain. Numerical computation is needed only to perform the final trace operation in J, which can be expressed as a two-dimensional integral in the Fourier domain. In addition, the SNR for the NPWMF can also be expressed in terms of scatter matrices. The problem is thus a useful way to gain facility in the use of the Hotelling formalism and shows its relation to the NPWMF.

The results show that the choice of task is important in assessing and optimizing imaging systems. If the task is detection of a known signal on a known uniform background, the pinhole size should be as large as possible. Similarly, both Wagner *et al.*[5] and Myers *et al.*[23] found that the high-contrast Rayleigh task was best performed by a large aperture. Obviously, these conclusions are not in accord with clinical experience in which some degree of spatial resolution is needed to perform realistic clinical tasks. In that respect, the stationary nonuniform background is more realistic and leads to the intuitively appealing conclusion that the aperture should be matched to the signals to be detected or discriminated. If the aperture is substantially smaller than the signal, photon collection suffers unnecessarily, while if it is much larger, the spatial resolution is inadequate for reliable discrimination between signal and background.

To summarize, this research has graphically demonstrated the limitations of too narrowly specifying the task in model calculations of the performance of imaging systems. Systems that work well, even optimally, on stylized tasks for which the background and the signal are both known exactly may fail badly with slightly more realistic tasks that include background variability.

APPENDIX A: DERIVATION OF THE COVARIANCE MATRIX

In this appendix we derive the covariance matrix of the data vector $\mathbf{g}$. We are concerned with a two-dimensional (planar) imaging system with planar objects and images. Nevertheless, we can represent two-dimensional objects and images as one-dimensional column vectors by lexicographically ordering their discretized values, so that the data vector $\mathbf{g}$ is related to the object vector $\mathbf{f}$ in the following way:

$$\mathbf{g} = \mathbf{H}\mathbf{f} + \mathbf{n}. \tag{A1}$$

If the data vector $\mathbf{g}$ and noise vector $\mathbf{n}$ are $M \times 1$ vectors, and the object vector $\mathbf{f}$ is an $N \times 1$ vector, then the system operator $\mathbf{H}$ is an $M \times N$ matrix. The system operator includes the aperture transmission function as well as the imaging geometry and exposure dependence [Eq. (2)].

The covariance matrix for the data vector $\mathbf{g}$, when class k ($k = 1, 2$) is true, is defined as

$$\mathbf{C}_k = \langle\langle(\mathbf{g} - \bar{\mathbf{g}}_k)(\mathbf{g} - \bar{\mathbf{g}}_k)^t\rangle_{n|f}\rangle_{f|k}, \tag{A2}$$

where $\bar{\mathbf{g}}_k$ is the mean image from class k, averaged over both the noise random variable $\mathbf{n}$, given an object $\mathbf{f}$, and the ensemble of objects $\mathbf{f}$ that belong to class k. The covariance matrix $\mathbf{C}_k$ characterizes the variation in the data due to the spatially varying object and the Poisson noise. The inhomogeneous background in the object is assumed to be stationary and independent of the signal. For low-contrast signals, then, $\mathbf{C}_k$ characterizes the same nonuniformity in the background and Poisson noise regardless of the class, so we can drop the subscript k from the covariance matrix ($\mathbf{C}_1 \simeq \mathbf{C}_2 \simeq \mathbf{C}$).

To determine $\mathbf{C}$, we add and subtract $\bar{\mathbf{g}}_f$, the mean data vector averaged over the Poisson noise for a given object $\mathbf{f}$, from each factor in Eq. (A2):

$$\mathbf{C} = \langle\langle(\mathbf{g} - \bar{\mathbf{g}}_f + \bar{\mathbf{g}}_f - \bar{\mathbf{g}})(\mathbf{g} - \bar{\mathbf{g}}_f + \bar{\mathbf{g}}_f - \bar{\mathbf{g}})^t\rangle_{n|f}\rangle_f. \tag{A3}$$

Equation (A3) may be rewritten as a sum of four matrices $\mathbf{M}_1$, $\mathbf{M}_2$, $\mathbf{M}_3$, and $\mathbf{M}_4$, with

$$\mathbf{M}_1 = \langle\langle(\mathbf{g} - \bar{\mathbf{g}}_f)(\mathbf{g} - \bar{\mathbf{g}}_f)^t\rangle_{n|f}\rangle_f, \tag{A4}$$

$$\mathbf{M}_2 = \langle\langle(\mathbf{g} - \bar{\mathbf{g}}_f)(\mathbf{g} - \bar{\mathbf{g}}_f)^t\rangle_{n|f}\rangle_f, \tag{A5}$$

$$\mathbf{M}_3 = -\langle\langle(\mathbf{g} - \bar{\mathbf{g}}_f)(\mathbf{g} - \bar{\mathbf{g}}_f)^t\rangle_{n|f}\rangle_f, \tag{A6}$$

$$\mathbf{M}_4 = -\langle\langle(\mathbf{g} - \bar{\mathbf{g}}_f)(\mathbf{g} - \bar{\mathbf{g}}_f)^t\rangle_{n|f}\rangle_f. \tag{A7}$$

To evaluate each of these matrices, let us call $M_l(i, j)$ (with $l = 1, 2, 3, 4$) the (i, j)th matrix element of $\mathbf{M}_l$. In addition, let us write $\langle g(i)\rangle_{n|f}$, the average data value at the ith pixel given the object $\mathbf{f}$, as $\bar{g}_f(i)$. In component form Eq. (A4) becomes

$$M_1(i, j) = \langle\langle[g(i) - \bar{g}_f(i)][g(j) - \bar{g}_f(j)]\rangle_{n|f}\rangle_f, \tag{A8}$$

which, for Poisson (independent) noise, and for $i \neq j$, becomes

$$\begin{aligned} M_1(i, j) &= \langle\langle g(i) - \bar{g}_f(i)\rangle_{n|f}\langle g(j) - \bar{g}_f(j)\rangle_{n|f}\rangle_f \\ &= 0, \qquad i \neq j. \end{aligned} \tag{A9}$$

For $i = j$, the matrix element $M_1(i, j) = M_1(i, i)$ is given by

$$\begin{aligned} M_1(i, i) &= \langle\langle[g(i) - \bar{g}_f(i)]^2\rangle_{n|f}\rangle_f \\ &= \langle\bar{g}_f(i)\rangle_f \\ &= \bar{g}(i) \\ &= \kappa A_{ap}\bar{B}. \end{aligned} \tag{A10}$$

We have again made the low-contrast assumption, so that the stationary background gives a mean pixel value in the image that is independent of position. The value $\bar{B}$ is the mean background level in the object, κ is the imaging parameter defined in Eq. (3), and A_{ap} is the area of the aperture ($A_{ap} = L^2$ for the square and $A_{ap} = 2\pi\sigma_p^2$ for the Gaussian aperture).

If we denote the autocorrelation function of the nonuniform background after the imaging process by $\mathbf{R}_g$, $M_2(i, j)$, $M_3(i, j)$, and $M_4(i, j)$ are given for any (i, j) by

$$\begin{aligned} M_2(i, j) &= \langle\langle[g(i) - \bar{g}_f(i)][g(j) - \bar{g}_f(j)]\rangle_{n|f}\rangle_f \\ &= \langle[g(i) - \bar{g}_f(i)][g(j) - \bar{g}_f(j)]\rangle_f \\ &= R_g(i, j), \end{aligned} \tag{A11}$$

$$\begin{aligned} M_3(i, j) &= \langle\langle[g(i) - \bar{g}_f(i)][g(j) - \bar{g}_f(j)]\rangle_{n|f}\rangle_f \\ &= \langle[g(i) - \bar{g}_f(i)]\langle[g(j) - \bar{g}_f(j)]\rangle_{n|f}\rangle_f \\ &= 0, \end{aligned} \tag{A12}$$

$$\begin{aligned} M_4(i, j) &= \langle\langle[g(i) - \bar{g}_f(i)][g(j) - \bar{g}_f(j)]\rangle_{n|f}\rangle_f \\ &= \langle\langle[g(i) - \bar{g}_f(i)]\rangle_{n|f}[g(j) - \bar{g}_f(j)]\rangle_f \\ &= 0. \end{aligned} \tag{A13}$$

We can now combine Eqs. (A9)–(A13) to write the (i, j)th element of the covariance matrix defined by Eq. (A2) as a sum of two terms:

$$C(i, j) = R_g(i, j) + \kappa A_{ap}\bar{B}\delta_{ij}, \tag{A14}$$

where δ_{ij} is the Kronecker delta function. The autocorrelation function of the nonuniform background in the image plane $\mathbf{R}_g$ is related to the autocorrelation function of the nonuniform background in the object plane $\mathbf{R}_f$ through a double convolution with the aperture function. Equation (A14) shows that the contributions of the Poisson noise and the nonuniform-background randomness to the covariance matrix of the data are additive.

APPENDIX B: DERIVATION OF THE HOTELLING SIGNAL-TO-NOISE RATIO

This appendix derives the continuous Fourier-domain representation of the Hotelling SNR. From Eq. (24) we can write the discrete space-domain representation of the Hotelling SNR:

$$\mathrm{SNR}^2_{\mathrm{Hot}} = \Delta\mathbf{s}^t\mathbf{H}^t\mathbf{C}^{-1}\mathbf{H}\Delta\mathbf{s}, \tag{B1}$$

where $\mathbf{C}$ is the covariance matrix of the data derived in Appendix A:

$$C(i, j) = R_g(i, j) + \kappa A_{ap}\bar{B}\delta_{ij}. \tag{B2}$$

We may simplify the calculation of $\mathrm{SNR}_{\mathrm{Hot}}$ by noting that under the assumption of a stationary background, the covariance matrix may be approximated by a circulant matrix, which is diagonalized by a discrete Fourier transform. We shall therefore calculate $\mathrm{SNR}_{\mathrm{Hot}}$ in the Fourier domain.

We shall represent the discrete Fourier operator by $\mathbf{F}$. We use $\mathbf{F}$ to map the difference signal $\Delta\mathbf{s}$ into the Fourier domain as follows:

$$\mathbf{F}\Delta\mathbf{s} = \Delta\tilde{\mathbf{s}}, \tag{B3}$$

where $\Delta\tilde{s}(m)$ is the Fourier amplitude of $\Delta\mathbf{s}$ at frequency ρ_m. Note that the Fourier operator as we have defined it maps a lexicographically ordered vector from the space domain to a lexicographically ordered vector in the Fourier domain. The Fourier operator $\mathbf{F}$ is a unitary operator, so that $\mathbf{F}\mathbf{F}^\dagger = \mathbf{F}^\dagger\mathbf{F} = \mathbf{I}$, where $\mathbf{I}$ is the identity matrix and the dagger represents the conjugate transpose of a matrix or vector. Since the difference signal is real, we find that

$$\Delta\tilde{\mathbf{s}}^\dagger = (\mathbf{F}\Delta\mathbf{s})^\dagger = \Delta\mathbf{s}^t\mathbf{F}^\dagger. \tag{B4}$$

We assume that the imaging process is linear and shift invariant. A shift-invariant imaging system can be represented by a system matrix $\mathbf{H}$ that is approximately circulant and, therefore, diagonalized by the discrete Fourier operator:

$$\mathbf{F}\mathbf{H}\mathbf{F}^\dagger = \tilde{\mathbf{H}}, \tag{B5}$$

with

$$\tilde{H}(i, j) = \tilde{H}(i)\delta_{ij}. \tag{B6}$$

We have written the diagonal matrix $\tilde{\mathbf{H}}$ in component form as a function of a single index that runs along the matrix diagonal.

In the Fourier domain the covariance matrix $\mathbf{C}$ becomes

$$\mathbf{F}\mathbf{C}\mathbf{F}^\dagger = \tilde{\mathbf{C}}, \tag{B7}$$

which we can write in component form as

$$\begin{aligned} \tilde{C}(i, j) &= [W_g(i) + \kappa A_{ap}\bar{B}]\delta_{ij} \\ &= [|\tilde{H}(i)|^2 W_f(i) + \kappa A_{ap}\bar{B}]\delta_{ij} \end{aligned} \tag{B8}$$

by using Eq. (B2). $\mathbf{W}_g$ is the power spectrum of the nonuniform background in the image plane, and $\mathbf{W}_f$ is the power spectrum of the nonuniform background in the object plane.

We can now write an equivalent expression for SNR_{Hot} in the Fourier domain by inserting Fourier operators as shown below:

$$\begin{aligned}SNR_{Hot}^2 &= \Delta\mathbf{s}^t\mathbf{H}^t\mathbf{C}^{-1}\mathbf{H}\Delta\mathbf{s}\\ &= \Delta\mathbf{s}^t(\mathbf{F}^\dagger\mathbf{F})\mathbf{H}^t(\mathbf{F}^\dagger\mathbf{F})\mathbf{C}^{-1}(\mathbf{F}^\dagger\mathbf{F})\mathbf{H}(\mathbf{F}^\dagger\mathbf{F})\Delta\mathbf{s}\\ &= (\Delta\mathbf{s}^t\mathbf{F}^\dagger)(\mathbf{F}\mathbf{H}^t\mathbf{F}^\dagger)(\mathbf{F}\mathbf{C}^{-1}\mathbf{F}^\dagger)(\mathbf{F}\mathbf{H}\mathbf{F}^\dagger)(\mathbf{F}\Delta\mathbf{s})\\ &= \Delta\tilde{\mathbf{s}}^\dagger\tilde{\mathbf{H}}^\dagger\tilde{\mathbf{C}}^{-1}\tilde{\mathbf{H}}\Delta\tilde{\mathbf{s}}. \end{aligned} \tag{B9}$$

In component form, this is written as

$$\begin{aligned}SNR_{Hot}^2 &= \sum_i\sum_j\sum_k\sum_l \Delta\tilde{s}^*(i)\tilde{H}^*(i,j)\tilde{C}^{-1}(j,k)\tilde{H}(k,l)\Delta\tilde{s}(l)\\ &= \sum_i \Delta\tilde{s}^*(i)\tilde{H}^*(i)\tilde{C}^{-1}(i)\tilde{H}(i)\Delta\tilde{s}(i)\\ &= \sum_i \frac{|\Delta\tilde{s}(i)|^2|\tilde{H}(i)|^2}{[\tilde{C}(i)]}\\ &= \sum_i \frac{|\Delta\tilde{s}(i)|^2|\tilde{H}(i)|^2}{[\kappa A_{ap}\bar{B} + |\tilde{H}(i)|^2W_f(i)]}, \end{aligned} \tag{B10}$$

where the superscript asterisk denotes the complex conjugate and we have made use of the delta functions in the diagonal matrices to reduce the multiple sum to a sum over a single index.

We can write SNR_{Hot} as a continuous integral in the Fourier domain by taking the limit of the sum for a large number of fine samples and undoing the lexicographic ordering to turn the one-dimensional sum back into a two-dimensional integral:

$$SNR_{Hot}^2 = \int_\infty d^2(\rho)\,\frac{|\Delta\tilde{s}(\rho)|^2|\tilde{H}(\rho)|^2}{[\kappa A_{ap}\bar{B} + |\tilde{H}(\rho)|^2W_f(\rho)]}. \tag{B11}$$

APPENDIX C: DERIVATION OF THE NONPREWHITENING MATCHED FILTER SIGNAL-TO-NOISE RATIO

The figure of merit for the NPWMF is the SNR associated with the NPWMF test statistic. The NPWMF test statistic was shown in Eq. (27) to be

$$\lambda_{npw} = \Delta\mathbf{s}^t\mathbf{H}^t\mathbf{g}. \tag{C1}$$

Since in this appendix we shall discuss only the test statistic for the NPWMF, we shall drop the subscript from the test statistic.

If we define $\bar{\lambda}_1$ and $\bar{\lambda}_2$ as the mean values of λ for classes 1 and 2, respectively, and σ_1^2 and σ_2^2 are its respective variances, the SNR associated with the test statistic is

$$SNR_{npw}^2 = \frac{(\bar{\lambda}_2 - \bar{\lambda}_1)^2}{\frac{1}{2}(\sigma_1^2 + \sigma_2^2)}. \tag{C2}$$

The mean and the variances are found by averaging over both the Poisson noise and the object variability due to the nonuniform background. In the low-contrast limit the variances are the same for both classes ($\sigma_1^2 \simeq \sigma_2^2 \simeq \sigma$), and Eq. (C2) becomes

$$SNR_{npw}^2 = \frac{[\Delta\bar{\lambda}]^2}{\sigma^2}. \tag{C3}$$

Let us consider the numerator first. The mean of λ when class k is true is

$$\bar{\lambda}_k = \langle\langle\lambda\rangle_{n|f}\rangle_{f|k}. \tag{C4}$$

We find the average for the class by performing an average over the Poisson noise for a particular object in the class, followed by an average over all objects from the class. If we use the expression for the test statistic in Eq. (C1) we find that

$$\begin{aligned}\bar{\lambda}_k &= \Delta\mathbf{s}^t\mathbf{H}^t\langle\langle\mathbf{g}\rangle_{n|f}\rangle_{f|k}\\ &= \Delta\mathbf{s}^t\mathbf{H}^t\bar{\mathbf{g}}_k. \end{aligned} \tag{C5}$$

The difference in the means of λ under the two hypotheses is then

$$\Delta\bar{\lambda} = \Delta\mathbf{s}^t\mathbf{H}^t\Delta\mathbf{g}. \tag{C6}$$

Moreover, by noting that $\Delta\mathbf{g}$ is simply the image of the difference signal, Eq. (C6) yields

$$\Delta\bar{\lambda} = \Delta\mathbf{s}^t\mathbf{H}^t\mathbf{H}\Delta\mathbf{s}. \tag{C7}$$

We calculate the variance of the test statistic by cascading averages over noise and objects in a similar manner. The definition of the variance of λ is

$$\sigma^2 = \langle\langle(\lambda - \bar{\lambda})^2\rangle_{n|f}\rangle_f. \tag{C8}$$

If we add and subtract the mean of λ for a particular object (averaged over the Poisson noise), Eq. (C8) becomes

$$\begin{aligned}\sigma^2 &= \langle\langle(\lambda - \bar{\lambda}_f + \bar{\lambda}_f - \bar{\lambda})^2\rangle_{n|f}\rangle_f\\ &= \langle\langle(\lambda - \bar{\lambda}_f)^2\rangle_{n|f}\rangle_f + \langle\langle(\bar{\lambda}_f - \bar{\lambda})^2\rangle_{n|f}\rangle_f. \end{aligned} \tag{C9}$$

A quick inspection will show that the cross term is equal to zero, and so we are left with two terms to evaluate. We evaluate the first term to find that

$$\begin{aligned}\langle\langle(\lambda - \bar{\lambda}_f)^2\rangle_{n|f}\rangle_f &= \langle\langle(\Delta\mathbf{s}^t\mathbf{H}^t\mathbf{g} - \Delta\mathbf{s}^t\mathbf{H}^t\bar{\mathbf{g}}_f)^2\rangle_{n|f}\rangle_f\\ &= \langle\langle\Delta\mathbf{s}^t\mathbf{H}^t(\mathbf{g} - \bar{\mathbf{g}}_f)(\mathbf{g} - \bar{\mathbf{g}}_f)^t\mathbf{H}\Delta\mathbf{s}\rangle_{n|f}\rangle_f\\ &= \Delta\mathbf{s}^t\mathbf{H}^t\langle\langle(\mathbf{g} - \bar{\mathbf{g}}_f)(\mathbf{g} - \bar{\mathbf{g}}_f)^t\rangle_{n|f}\rangle_f\mathbf{H}\Delta\mathbf{s}\\ &= \Delta\mathbf{s}^t\mathbf{H}^t\mathbf{M}_1\mathbf{H}\Delta\mathbf{s}, \end{aligned} \tag{C10}$$

where the diagonal matrix $\mathbf{M}_1$ characterizes the contribution of the Poisson noise to the variance and is shown in Appendix A [Eqs. (A9) and (A10)] to be given by

$$\mathbf{M}_1 = \kappa A_{ap}\bar{B}\mathbf{I} \tag{C11}$$

in the low-contrast limit, where $\mathbf{I}$ is the identity matrix.

The second term in Eq. (C9) is given by

$$\begin{aligned}\langle\langle(\bar{\lambda}_f - \bar{\lambda})^2\rangle_{n|f}\rangle_f &= \langle\langle(\Delta\mathbf{s}^t\mathbf{H}^t\bar{\mathbf{g}}_f - \Delta\mathbf{s}^t\mathbf{H}^t\bar{\mathbf{g}})^2\rangle_{n|f}\rangle_f\\ &= \Delta\mathbf{s}^t\mathbf{H}^t\langle\langle(\bar{\mathbf{g}}_f - \bar{\mathbf{g}})(\bar{\mathbf{g}}_f - \bar{\mathbf{g}})^t\rangle_{n|f}\rangle_f\mathbf{H}\Delta\mathbf{s}\\ &= \Delta\mathbf{s}^t\mathbf{H}^t\mathbf{R}_g\mathbf{H}\Delta\mathbf{s}, \end{aligned} \tag{C12}$$

where $\mathbf{R}_g$ is the autocorrelation function of the nonuniform background in the image plane.

We can now combine the expressions for the mean and the variance to write $\mathrm{SNR}^2_{\mathrm{npw}}$:

$$\mathrm{SNR}^2_{\mathrm{npw}} = \frac{(\Delta \mathbf{s}^t \mathbf{H}^t \mathbf{H} \Delta \mathbf{s})^2}{\Delta \mathbf{s}^t \mathbf{H}^t (\kappa A_{\mathrm{ap}} \bar{B} \mathbf{I} + \mathbf{R}_g) \mathbf{H} \Delta \mathbf{s}}. \tag{C13}$$

This expression may be simplified by performing the calculation in the Fourier domain, using the scheme presented in Appendix B. The Fourier-domain representation is then shown to be

$$\mathrm{SNR}^2_{\mathrm{npw}} = \frac{(\Delta \tilde{\mathbf{s}}^\dagger \tilde{\mathbf{H}}^\dagger \tilde{\mathbf{H}} \Delta \tilde{\mathbf{s}})^2}{\Delta \tilde{\mathbf{s}}^\dagger \tilde{\mathbf{H}}^\dagger (\kappa A_{\mathrm{ap}} \bar{B} \mathbf{I} + \mathbf{W}_g) \tilde{\mathbf{H}} \Delta \tilde{\mathbf{s}}}. \tag{C14}$$

If we write out the summations represented implicitly in the matrix notation, we find that

$$\begin{aligned} \mathrm{SNR}^2_{\mathrm{npw}} &= \frac{\left[\sum_i |\Delta \tilde{s}(i)|^2 |\tilde{H}(i)|^2 \right]^2}{\sum_i |\Delta \tilde{s}(i)|^2 |\tilde{H}(i)|^2 [\kappa A_{\mathrm{ap}} \bar{B} + W_g(i)]} \\ &= \frac{\left[\sum_i |\Delta \tilde{s}(i)|^2 |\tilde{H}(i)|^2 \right]^2}{\sum_i |\Delta \tilde{s}(i)|^2 |\tilde{H}(i)|^2 [\kappa A_{\mathrm{ap}} \bar{B} + |\tilde{H}(i)|^2 W_f(i)]}. \end{aligned} \tag{C15}$$

In the limit in which the area of the sampling element approaches zero, the discrete sums approximate integrals, and Eq. (C15) becomes

$$\mathrm{SNR}^2_{\mathrm{npw}} = \frac{I_1^2}{\kappa A_{\mathrm{ap}} \bar{B} I_1 + I_2}, \tag{C16}$$

where, if $\boldsymbol{\rho}$ is the two-dimensional spatial-frequency vector,

$$I_1 = \int_\infty \mathrm{d}^2 \rho |\Delta \tilde{s}(\boldsymbol{\rho})|^2 |\tilde{H}(\boldsymbol{\rho})|^2 \tag{C17}$$

and

$$I_2 = \int_\infty \mathrm{d}^2 \rho |\Delta \tilde{s}(\boldsymbol{\rho})|^2 |\tilde{H}(\boldsymbol{\rho})|^4 W_f(\boldsymbol{\rho}). \tag{C18}$$

ACKNOWLEDGMENTS

The authors have benefitted greatly from discussions with D. G. Brown. This research was supported in part by the National Institutes of Health under grant PO1 CA 23417.

REFERENCES

1. H. H. Barrett and W. Swindell, *Radiological Imaging: The Theory of Image Formation, Detection and Processing* (Academic, New York, 1981).
2. H. L. Van Trees, *Detection, Estimation, and Modulation Theory* (Wiley, New York, 1968), Vols. I, II, and III.
3. A. D. Whalen, *Detection of Signals in Noise* (Academic, New York, 1971).
4. B. M. W. Tsui, C. E. Metz, F. B. Atkins, S. J. Starr, and R. N. Beck, "A comparison of optimum spatial resolution in nuclear imaging based on statistical theory and on observer performance," Phys. Med. Biol. **23**, 654–676 (1978).
5. R. F. Wagner, D. G. Brown, and C. E. Metz, "On the multiplex advantage of coded source/aperture photon imaging," in *Digital Radiography*, W. Brody, ed., Proc. Soc. Photo-Opt. Instrum. Eng. **314**, 72–76 (1981).
6. J. L. Harris, "Resolving power and decision theory," J. Opt. Soc. Am. **54**, 606–611 (1964).
7. H. H. Barrett, "Objective assessment of image quality: effects of quantum noise and object variability," J. Opt. Soc. Am. A **7**, 1266–1278 (1990).
8. R. F. Wagner, K. J. Myers, D. G. Brown, M. J. Tapiovaara, and A. E. Burgess, "Higher-order tasks: human vs. machine performance," in *Medical Imaging III: Image Formation*, R. H. Schneider, S. J. Dwyer, and R. G. Jost, eds., Proc. Soc. Photo-Opt. Instrum. Eng. **1090**, 183–194 (1989).
9. H. Hotelling, "The generalization of Student's ratio," Ann. Math. Stat. **2**, 360 (1931).
10. K. Fukunaga, *Introduction to Statistical Pattern Recognition* (Academic, New York, 1972).
11. H. H. Barrett, W. E. Smith, K. J. Myers, T. D. Milster, and R. D. Fiete, "Quantifying the performance of imaging systems," in *Application of Optical Instrumentation in Medicine XIII*, R. H. Schneider and S. J. Dwyer, eds., Proc. Soc. Photo-Opt. Instrumen. Eng. **535**, 65–69 (1985).
12. H. H. Barrett, K. J. Myers, and R. F. Wagner, "Beyond signal-detection theory," in *Application of Optical Instrumentation in Medicine XIV*, R. H. Schneider and S. J. Dwyer, eds., Proc. Soc. Photo-Opt. Instrum. Eng. **626**, 231–239 (1986).
13. W. E. Smith and H. H. Barrett, "The Hotelling trace criterion as a figure of merit for the optimization of imaging systems," J. Opt. Soc. Am. A **3**, 717–725 (1986).
14. R. D. Fiete, H. H. Barrett, W. E. Smith, and K. J. Myers, "The Hotelling trace criterion and its correlation with human observer performance," J. Opt. Soc. Am. A **4**, 945–953 (1987).
15. J. P. Rolland, *Factors Influencing Lesion Detectability in Medical Imaging*, Ph.D. dissertation (University of Arizona, Tucson, Ariz., 1990).
16. Z. H. Gu and S. Lee, "Optical implementation of the Hotelling trace criterion for image classification," Opt. Eng. **23**, 727–731 (1984).
17. H. H. Barrett, J. P. Rolland, R. F. Wagner, and K. J. Myers, "Detection and discrimination of known signals in inhomogeneous random backgrounds," in *Medical Imaging III: Image Formation*, R. H. Schneider, S. J. Dwyer, and R. G. Jost, eds., Proc. Soc. Photo-Opt. Instrum. Eng. **1090**, 176–182 (1989).
18. R. Shaw, "Evaluating the efficiency of imaging processes," Rep. Prog. Phys. **41**, 1103–1155 (1978).
19. J. C. Dainty and R. Shaw, *Image Science* (Academic, London, 1974).
20. R. F. Wagner and D. G. Brown, "Unified SNR analysis of medical imaging systems," Phys. Med. Biol. **30**, 489–518 (1985).
21. A. E. Burgess, R. F. Wagner, R. J. Jennings, and H. B. Barlow, "Efficiency of human visual discrimination," Science **214**, 93–94 (1981).
22. K. J. Myers, H. H. Barrett, M. C. Borgstrom, D. D. Patton, and G. W. Seeley, "Effect of noise correlation on detectability of disk signals in medical imaging," J. Opt. Soc. Am. A **2**, 1752–1759 (1985).
23. K. J. Myers, R. F. Wagner, D. G. Brown, and H. H. Barrett, "Efficient utilization of aperture and detector by optimal coding," in *Medical Imaging III: Image Formation*, R. H. Schneider, S. J. Dwyer, and R. G. Jost, eds., Proc. Soc. Photo-Opt. Instrum. Eng. **1090**, 164–175 (1989).
24. K. M. Hanson, "Method of evaluating image-recovery algorithms based on task performance," J. Opt. Soc. Am. A **7**, 1294–1304 (1990).